Comparison of force sensors for atomic force microscopy based on quartz tuning forks and length-extensional resonators

Franz J. Giessibl* and Florian Pielmeier
Universität Regensburg, Institute of Experimental and Applied Physics, Universitätsstrasse 31, D-93040 Regensburg, Germany

Toyoaki Eguchi†
NAKAJIMA Designer Nanocluster Assembly Project, ERATO, Japan Science and Technology Agency (JST), 3-2-1 Sakato, Takatsu-ku, Kawasaki 213-0012, Japan and Graduate School of Science and Technology, Keio University, 3-14-1 Hiyoshi, Kohoku-ku, Yokohama 223-8522, Japan

Toshu An
Institute for Materials Research, Tohoku University, 2-1-1, Katahira, Aoba-ku, Sendai 980-8577, Japan

Yukio Hasegawa
Institute for Solid State Physics, University of Tokyo 5-1-5, Kashiwa-no-ha, Kashiwa, Chiba 277-8581, Japan
(Received 14 April 2011; revised manuscript received 15 July 2011; published 6 September 2011)

The force sensor is key to the performance of atomic force microscopy (AFM). Nowadays, most atomic force microscopes use micromachined force sensors made from silicon, but piezoelectric quartz sensors are being applied at an increasing rate, mainly in vacuum. These self-sensing force sensors allow a relatively easy upgrade of a scanning tunneling microscope to a combined scanning tunneling/atomic force microscope. Two fundamentally different types of quartz sensors have achieved atomic resolution: the "needle sensor," which is based on a length-extensional resonator, and the "qPlus sensor," which is based on a tuning fork. Here, we calculate and measure the noise characteristics of these sensors. We find four noise sources: deflection detector noise, thermal noise, oscillator noise, and thermal drift noise. We calculate the effect of these noise sources as a factor of sensor stiffness, bandwidth, and oscillation amplitude. We find that for self-sensing quartz sensors, the deflection detector noise is independent of sensor stiffness, while the remaining three noise sources increase strongly with sensor stiffness. Deflection detector noise increases with bandwidth to the power of 1.5, while thermal noise and oscillator noise are proportional to the square root of the bandwidth. Thermal drift noise, however, is inversely proportional to bandwidth. The first three noise sources are inversely proportional to amplitude while thermal drift noise is independent of the amplitude. Thus, we show that the earlier finding that quoted an optimal signal-to-noise ratio for oscillation amplitudes similar to the range of the forces is still correct when considering all four frequency noise contributions. Finally, we suggest how the signal-to-noise ratio of the sensors can be improved further, we briefly discuss the challenges of mounting tips, and we compare the noise performance of self-sensing quartz sensors and optically detected Si cantilevers.

DOI: 10.1103/PhysRevB.84.125409 PACS number(s): 68.37.Ps, 07.79.Lh, 34.20.−b

I. INTRODUCTION

Atomic force microscopy (AFM) was introduced in 1986 by Binnig, Gerber, and Quate.[1] The large number of citations (the article is now one of the most highly cited publications to have appeared in *Physical Review Letters*) show that AFM is an important scientific tool with fruitful applications in various fields of science. The key element of AFM is the force sensor that probes the small forces that act between a sharp tip and a sample. Simplifying the force sensor and increasing its force resolution and imaging speed are therefore important tasks.

Atomic resolution by AFM on a reactive surface was first achieved by frequency modulation AFM (FM-AFM)[2] utilizing a piezoresistive silicon cantilever[3] with a spring constant of $k = 17$ N/m at an oscillation amplitude of $A = 34$ nm.[4] While atomic resolution on various surfaces has been obtained with similar combinations of (k,A) (see Table I in Ref. 5), a calculation of the signal-to-noise ratio in FM-AFM as a function of the oscillation amplitudes yielded an optimal oscillation amplitude that corresponds to the decay length of the forces that are used for imaging. The spring constant of the cantilever should be as small as possible to obtain a large frequency shift; on the other hand, the cantilever must be stiff enough to prevent instabilities such as jump-to-contact.[6] Compared to the initial parameter set of (k,A) that allowed atomic resolution,[4] the spring constant of the sensor has to be larger by a factor of about one to two orders of magnitude, and the amplitude has to be reduced by a factor of two to three orders of magnitude. The reduced amplitude not only increases the signal-to-noise ratio, it also reduces the sensitivity to unwanted long-range force contributions.[5] Figure 1 shows the parameters used with "classic" Si cantilevers, qPlus sensors, and needle sensors.

For atomic imaging, it was suggested that the optimal stiffness k_{opt} is approximately in the interval

$$500 < k_{\mathrm{opt}} < 3000 \text{ N/m} \quad (1)$$

at amplitudes of about 100 pm.[6]

Self-sensing cantilevers such as piezoresistive silicon cantilevers or piezoelectric quartz sensors are attractive because these sensors simply need to be connected to an electronic

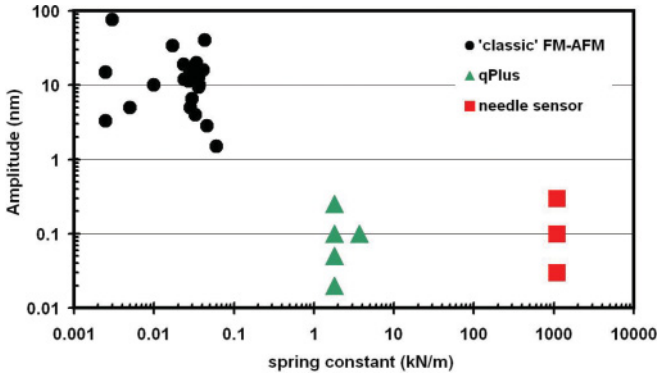

FIG. 1. (Color online) Parameter fields of cantilever spring constants k and oscillation amplitudes A for classic Si cantilevers, qPlus sensors, and needle sensors. The (k,A) data points for Si cantilevers and qPlus sensors are adapted from Table I in Ref. 5, and those from shortened qPlus sensors are taken from Ref. 7. To enable stable oscillation of the cantilever at the optimal amplitudes around 100 pm, it was necessary to increase the spring constants of cantilevers ("classic" FM-AFM) from about 10 N/m by more than two orders of magnitude (qPlus sensors). The needle sensor has a stiffness that is almost three orders of magnitude larger than that of the qPlus sensor. The question of whether this further increase is beneficial is addressed in this paper.

preamplifier to provide an electrical deflection signal. In contrast, sensors that utilize deflection measurements based on electron tunneling[1] or optical means[8] require precise mechanical alignment schemes that can be challenging in vacuum or low-temperature environments. Optical deflection measurements also involve light and heat introduction close to the sample. For some applications, such as low-temperature measurements or the study of samples that alter their properties under electromagnetic radiation, optical deflection measurements are disadvantageous.

Because FM-AFM relies on the alteration of the oscillation frequency of the cantilever under the influence of tip-sample force gradients, a high intrinsic frequency stability of the cantilever is desirable. Silicon cantilevers, the most widespread type in use, change their frequency by -35 ppm per K at room temperature.[9] In contrast, quartz resonators change their frequency by less than 1 ppm per K as long as their temperature is kept within ± 14 K of their turnover temperature [see Eq. (47)]. The outstanding stability of quartz that has been utilized for decades for watches and frequency standards provides for highly stable FM-AFM sensors as well.

Two types of commercially available quartz frequency standards are particularly well suited for conversion into force sensors: quartz tuning forks and length-extensional resonators (LER's). Both tuning forks and LER's essentially consist of two coupled electromechanical oscillators that have exactly the same eigenfrequency and oscillate in an antiparallel mode. Attaching a tip to one of the oscillators changes its resonance frequency, so the tip either has to be very light or a similar mass has to be attached to the other oscillator. Force sensors based on tuning forks were already used by Guethner *et al.*[10] in 1989, when a tip was mounted onto one prong and the mass of the tip was balanced with a counterweight on the other prong.[11] The LER was supplemented by a light tip on one of its two bars to form the needle sensor after the work of Bartzke *et al.*[12,13] in 1993. The qPlus sensor is also based on a tuning fork, but one of the prongs is immobilized by attaching it to a heavy substrate such that the free prong is essentially a quartz cantilever.[14–16] In this case, the tip can be massive, and the oscillating tip can interact vigorously with the sample without a reduction in the Q value. These sensors with metal probe tips allow a simple implementation of combined scanning tunneling microscopy (STM) and AFM. Quartz tuning forks are available with eigenfrequencies f_0 ranging from about 32 to 200 kHz. LER's are available in eigenfrequencies of 0.5 MHz to a few MHz.[17] In the comparison here, we focus on a specific type of tuning fork that is used in SWATCH wristwatches with stiffness $k' = 1800$ N/m and $f_0 = 32\,768$ Hz and a specific type of LER with $k' = 540$ kN/m and $f_0 = 1$ MHz, because these types were used in the experimental data cited below (see Fig. 3 and Table I for geometric details). In Sec. VII, we will suggest optimized geometries for both types of sensors, but here we refer to a "standard qPlus sensor" or a "standard needle sensor" as shown in Fig. 2 to be based on the geometries as specified in Table I.

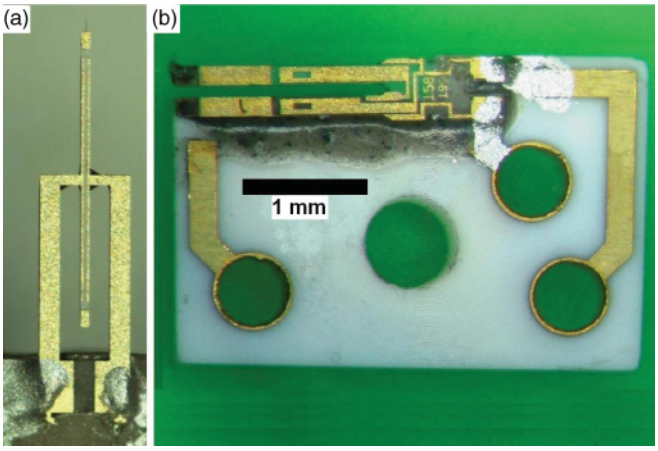

FIG. 2. (Color online) (a) Needle sensor. (b) qPlus sensor. The scale bar is valid for both sensors.

A qPlus sensor with $k = 1.8$ kN/m has allowed subatomic spatial resolution,[18,19] atomic resolution of lateral forces,[20] simultaneous force and current spectroscopy on graphite,[21] the measurement of forces acting in atomic manipulation,[22] the detection of a single charge on an atom,[23] and unprecedented spatial resolution of an organic molecule,[24] and it helped to identify an initially unidentified organic molecule that was hauled up from the Mariana Trench.[25] Even more recently, the relationship between tunneling current and forces has been revealed[26] and the interaction of two CO molecules has been studied.[27] Furthermore, a reduction of the effective tunneling voltage caused by the flow of current on weakly conductive samples has been detected by a reduced electrostatic attraction.[28]

Although the needle sensor's effective stiffness of more than 1 MN/m [$k = 2k'$, see Eq. (16)] is far beyond the optimal stiffness range suggested above, it has produced atomic resolution on silicon at 4 K (Refs. 29 and 30) and at room temperature.[31] Therefore, it is instructive to analyze the success factors of these sensors for the purpose of further improving their performance.

TABLE I. Geometrical parameters, stiffness k, and eigenfrequency f_0 of the quartz oscillators used. The needle sensor is based on a length-extensional resonator, while the qPlus sensor is based on a quartz tuning fork.

	L (μm)	L_e (μm)	t (μm)	w (μm)	k' (N/m)	k (N/m)	f_0 (Hz)
Needle sensor	1340	1100	70	130	540 000	1 080 000	1 000 000
qPlus sensor	2400	1600	214	126	1800	1800	32 768

II. FREQUENCY SHIFT AS A FUNCTION OF TIP-SAMPLE INTERACTION FOR SINGLE AND COUPLED OSCILLATORS

In frequency modulation atomic force microscopy, the eigenfrequency f of a force sensor (such as a qPlus sensor or a needle sensor; see Fig. 3) that vibrates at a constant amplitude A changes with the action of force gradients by a frequency shift $\Delta f = f - f_0$. With $f = f_0 + \Delta f$ and $f_0 = \frac{1}{2\pi}\sqrt{k/m^*}$, the frequency shift is given by

$$\Delta f = \frac{f_0}{2k}\langle k_{\rm ts}\rangle \tag{2}$$

with[32]

$$\langle k_{\rm ts}\rangle(z) = \frac{2}{\pi}\int_{-1}^{1} k_{\rm ts}(z+\zeta A)\sqrt{1-\zeta^2}\,d\zeta. \tag{3}$$

At large amplitudes, the frequency shift is given by

$$\Delta f = \frac{f_0}{k}\frac{1}{A^{3/2}}\gamma_{\rm ts} \tag{4}$$

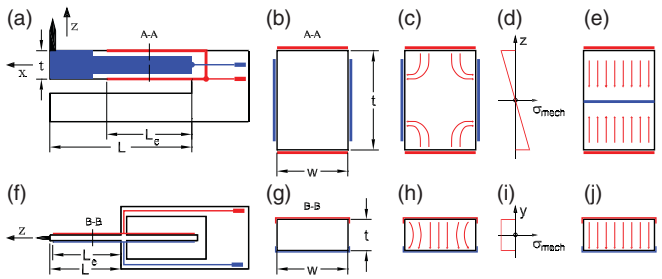

FIG. 3. (Color online) Geometry of sensors based on quartz tuning forks (a)–(e) and length-extensional resonators (f)–(j). A qPlus sensor (a) is created by attaching one of the prongs of the tuning fork to a substrate and attaching a tip to the other prong. For clarity, only the electrodes on the free prong are shown. The prong without displayed electrodes is fixed to a massive substrate (not shown here; see Fig. 2(b)). A needle sensor (f) is built by attaching a light tip to one prong of the length-extensional resonator. Parts (a), (b), (f), and (g) illustrate the geometrical dimensions as listed in Table I; parts (c) and (h) show a schematic view of the electrostatic field in the cross sections; and parts (d) and (i) show the mechanical stress profile along a cross section. Parts (e) and (j) show the idealized field distribution within the quartz crystals. The qPlus sensor uses a bending mode, thus the mechanical stress is maximal where the charge-collecting electrodes are located (d), while the length-extensional resonator develops a uniform stress profile (i). The idealized field distribution (e,j) is much closer to the actual field distribution (c,h) for the needle sensor [(j) vs (h)] than for the qPlus sensor [(e) vs (c)].

with the normalized frequency shift $\gamma_{\rm ts} \approx 0.4 F_{\rm ts}\sqrt{\lambda}$.[33] When A is very small compared to the decay length λ of the force gradient, $\langle k_{\rm ts}\rangle(z)$ is similar to $k_{\rm ts}(z)$, the gradient of the tip-sample forces at the center position of the cantilever that oscillates around $z \pm A$.

The eigenfrequency is found by solving the equation of motion for the cantilever deflection $q(t)$, the single degree of freedom (see Fig. 4(a))

$$m^*\frac{\partial^2 q}{\partial t^2} = -q(k + k_{\rm ts}) \tag{5}$$

resulting in $q(t) = A\cos(\omega t + \phi)$ with $\omega^2 = (k + k_{\rm ts})/m^*$ and $\omega = 2\pi f$.

Figure 4(b) shows a coupled oscillator such as a tuning fork or a LER. In the case of a coupled oscillator, the oscillator has three degrees of freedom $q_1(t)$, $q_2(t)$, and $q_c(t)$, leading to more complicated modes than in the case of a cantilever or qPlus sensor with its single degree of freedom. When the inertial forces (given by mass times acceleration) of the center piece of the LER can be neglected (a fair assumption for the antiparallel mode), the equation of motion is relatively easy to solve:

$$m^*\frac{\partial^2 q_1}{\partial t^2} = -k_{\rm ts}q_1 + k'(q_c - q_1), \tag{6}$$

$$m^*\frac{\partial^2 q_2}{\partial t^2} = -k'(q_2 - q_c). \tag{7}$$

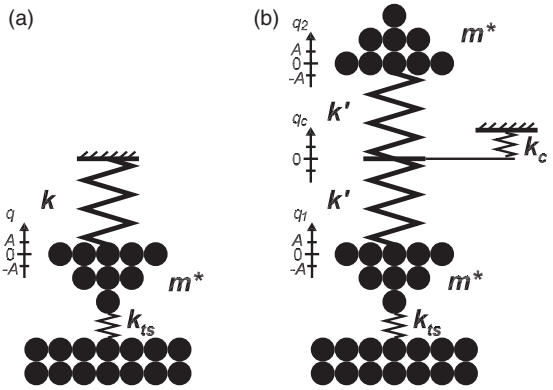

FIG. 4. (a) Mechanical analog of a single oscillator-type force sensor [standard cantilever or qPlus sensor as in Fig. 2(b)], consisting of a single oscillating beam. The single oscillator has only one degree of freedom, its deflection q. (b) Mechanical analog of a coupled oscillator used as a force sensor [tuning fork or length-extensional resonator as in Fig. 2(a)]. The coupled oscillator has three degrees of freedom: the deflection of the central mount q_c and the deflections of the two coupled oscillators $q_{1,2}$.

Because the center of the LER needs to be in equilibrium, we find

$$q_c k_c = k'(q_1 - q_c) + k'(q_2 - q_c). \tag{8}$$

With $\kappa = 1/(2 + k_c/k')$, we can substitute $q_c = \kappa(q_1 + q_2)$ and find

$$\frac{\partial^2 q_1}{\partial t^2} = -\omega_0^2(1 + k_{ts}/k' - \kappa)q_1 + \omega_0^2 \kappa q_2, \tag{9}$$

$$\frac{\partial^2 q_2}{\partial t^2} = +\omega_0^2 \kappa q_1 - \omega_0^2(1 - \kappa)q_2 \tag{10}$$

with $\omega_0^2 = k'/m^*$. Using a harmonic ansatz $q_{1,2}(t) = A_{1,2}\cos(\omega t + \phi_{1,2})$, we find two solutions for ω,

$$\omega_{1,2}^2 = \omega_0^2 \left\{ 1 - \kappa + \frac{k_{ts}}{2k'} \pm \sqrt{\kappa^2 + \frac{k_{ts}^2}{4k'^2}} \right\}. \tag{11}$$

Typically, $\kappa > 1/3$ because $k_c < k'$, and with $k_{ts} \ll k'$ we can approximate the square root in Eq. (11):

$$\omega_{1,2}^2 \approx \omega_0^2 \left\{ 1 - \kappa + \frac{k_{ts}}{2k'} \pm \kappa \left(1 + \frac{k_{ts}^2}{8\kappa^2 k'^2} \right) \right\}. \tag{12}$$

Two solutions are found, where the plus sign in Eq. (11) corresponds to a high-frequency antiparallel motion ($A_1 \approx -A_2, \phi_1 = \phi_2$),

$$\omega_1^2 \approx \omega_0^2 \left\{ 1 + \frac{k_{ts}}{2k'} + \frac{k_{ts}^2}{8\kappa k'^2} \right\}, \tag{13}$$

and the minus sign to a low-frequency parallel motion ($A_1 \approx A_2, \phi_1 = \phi_2$),

$$\omega_2^2 \approx \omega_0^2 \left\{ 1 - 2\kappa + \frac{k_{ts}}{2k'} - \frac{k_{ts}^2}{8\kappa k'^2} \right\}. \tag{14}$$

The antiparallel motion is used in force microscopy with coupled oscillators, where the frequency shift of the sensor is given by

$$\frac{\omega_1 - \omega_0}{\omega_0} = \frac{\Delta f}{f_0} = \frac{k_{ts}}{4k'} \tag{15}$$

(in leading order of k_{ts}). The frequency shift for a coupled oscillator is thus only half the value of the single oscillator after Eq. (2). We can still use Eqs. (2) and (4) by defining an effective stiffness k that is twice as large as the individual stiffness k' of each of the two coupled oscillators,

$$k_{\text{coupled}} = 2k'. \tag{16}$$

Equation (2) links the signal (i.e., the physical observable) to k_{ts}, the physical origin of the signal, by multiplying it with the prefactor $f_0/2k$. To obtain a strong signal, the prefactor $f_0/2k$ should be large. For a tip-sample force gradient of 1 N/m, a standard needle sensor would yield a frequency shift of $\Delta f = 0.463$ Hz, while a standard qPlus sensor would yield a frequency shift of $\Delta f = 8.33$ Hz. However, to assess the signal-to-noise ratio, we need to consider noise as well as signal strength. Noise also depends on the sensor type and will be discussed in Sec. V.

III. OPERATING PRINCIPLES AND SENSITIVITY OF QUARTZ SENSORS

A. Sensor based on quartz tuning fork (qPlus sensor)

For a rectangular cantilever with width w, thickness t, and length L, the spring constant k is given by[34]

$$k = \frac{E w t^3}{4L^3}, \tag{17}$$

where E is Young's modulus. The fundamental eigenfrequency f_0 is given by[34]

$$f_0 = 0.162 \frac{t}{L^2} v_s, \tag{18}$$

where v_s is the speed of sound in quartz as defined below.

The calculation of the sensitivity is slightly more complicated than in the case of the needle sensor. Here, we adapt the result from Ref. 16,

$$S_{\text{qPlus}}^{\text{theory}} = q_{\text{el}}/A = 12 d_{21} k \frac{L_e(L - L_e/2)}{t^2}. \tag{19}$$

Standard qPlus sensors with dimensions listed in Table I yield $S_{\text{qPlus}}^{\text{theory}} = 2.8\ \mu$C/m. It is important to note that the calculated sensitivity assumes a field distribution as shown in Fig. 3(e), while the actual field looks more like Fig. 3(c).

B. Sensor based on the length-extensional resonator (needle sensor)

The needle sensor consists of two coupled beams that oscillate opposite to each other [see Figs. 2(a) and 3(f)]. The longitudinal stiffness k' of each of the two bars that constitute the needle sensor is given by

$$k' = \frac{E w t}{L}, \tag{20}$$

with Young's modulus E, length L, width w, and thickness t of each quartz beam. The fundamental eigenmode is a longitudinal standing wave with a node at the root of each beam and its end at a maximal deflection, thus the length of one beam L corresponds to a quarter wavelength $\lambda/4$. Because the velocity of sound is $v_s = \sqrt{E/\rho}$ with mass density ρ, the eigenfrequency is given by

$$f_0 = \frac{v_s}{4L}. \tag{21}$$

The deflection of a cross section at a distance z from the mount is given by

$$\delta z(z) = A \sin\left(\frac{\pi z}{2L}\right) \tag{22}$$

when the ends of the device oscillate at amplitude A. The strain as a function of the z position is then given by

$$\epsilon(z) = \frac{\partial \delta z(z)}{\partial z} = \frac{\pi A}{2L} \cos\left(\frac{\pi z}{2L}\right). \tag{23}$$

The strain ϵ leads to a mechanical stress σ_{mech} given by

$$\sigma_{\text{mech}}(z) = E\epsilon(z). \tag{24}$$

The piezoelectric effect causes the emergence of a surface charge density σ_{el} given by

$$\sigma_{\text{el}}(z) = d_{21}\sigma_{\text{mech}}(z), \tag{25}$$

where $d_{21} = 2.31$ pC/N is the transverse piezoelectric coupling coefficient of quartz,[35] which is equal to the longitudinal piezoelectric coupling coefficient d_{11}. It is important to note that d_{21} is essentially constant over the temperature range from 1.5 K to room temperature.[35] When the charge density is integrated over the surface of the sensor, the total charge q_{el} at a given deflection A is given by

$$q_{\mathrm{el}} = d_{21} w \int_{-L_e}^{L_e} E \frac{A\pi}{2L} \cos\left(\frac{z\pi}{2L}\right) dz. \tag{26}$$

Thus, the sensitivity is given by

$$S_{\mathrm{LER}}^{\mathrm{theory}} = q_{\mathrm{el}}/A = 2 d_{21} E w \sin\left(\frac{L_e \pi}{2L}\right). \tag{27}$$

With Eq. (20), we can express Eq. (27) as

$$S_{\mathrm{LER}}^{\mathrm{theory}} = 2 d_{21} k' \frac{L}{t} \sin\left(\frac{\pi L_e}{2L}\right). \tag{28}$$

The electrodes extend almost to the end of the beams ($L_e = 1.1$ mm, $L = 1.34$ mm), therefore the sine in the equation above is almost 1 (exact value 0.960 685 188), and with $L/t = 1340/70$, we find $S_{\mathrm{LER}}^{\mathrm{theory}} \approx 19 \times d_{21} \times k'$. With the stiffness $k' = 540$ kN/m, we find a theoretical sensitivity of $S_{\mathrm{LER}}^{\mathrm{theory}} = 45\ \mu$C/m.

IV. SIGNAL

A. Frequency shift for exponential force laws and amplitude dependence of the signal-to-noise ratio

In FM-AFM, the signal is a frequency shift Δf. This frequency shift depends on the tip sample interaction and the stiffness k, eigenfrequency f_0, and amplitude A of the cantilever. For a force that follows an exponential distance dependence $F(z) = F_0 \exp(-\kappa z)$, we find

$$\Delta f = \frac{f_0}{kA} F_0 e^{-\kappa(z+A)} I_1(\kappa A), \tag{29}$$

where $I_1(\kappa A)$ is the Bessel function of the first kind, a special version of the Kummer function.[33]

As we will see below, the noise in the frequency measurement of the sensor is inversely proportional to A, therefore the signal-to-noise ratio (SNR) (see Fig. 5) can be expressed as

$$\mathrm{SNR} \propto e^{-\kappa A} I_1(\kappa A). \tag{30}$$

This function has its maximum at $\kappa A = 1.545\ldots$, thus the optimal SNR is reached for amplitudes that correspond to the decay length $\lambda = 1/\kappa$ of the tip-sample force,[6] or more precisely, $A_{\mathrm{opt}} \approx 1.545\lambda$. In theory, this ideal amplitude applies to all sensors in FM-AFM that probe interactions of range λ, provided the sensor stiffness is sufficient to enable stable oscillation close to the surface.[6]

We can rewrite Eq. (29) such that its resemblance to the gradient approximation becomes more clear:

$$\Delta f = \frac{f_0}{2k} \kappa F_0 e^{-\kappa z} \frac{2 I_1(\kappa A) e^{-\kappa A}}{\kappa A}. \tag{31}$$

The first factor in this equation is the gradient approximation, while the fraction $2I_1(x)e^{-x}/x$ with $x = \kappa A$ can be expanded as $2I_1(x)e^{-x}/x = 1 - x + 5/8x^2 + O(x^3)$. For a minimum distance between the tip and sample of z, the tip oscillates within the interval $[z \ldots z + 2A]$, and at the optimal oscillation amplitude $A_{\mathrm{opt}} \approx 1.545/\kappa$, we obtain an average tip-sample force gradient that is approximately one-third of the peak force gradient at distance z, because $2I_1(1.545)e^{-1.545}/1.545 \approx 0.33$.

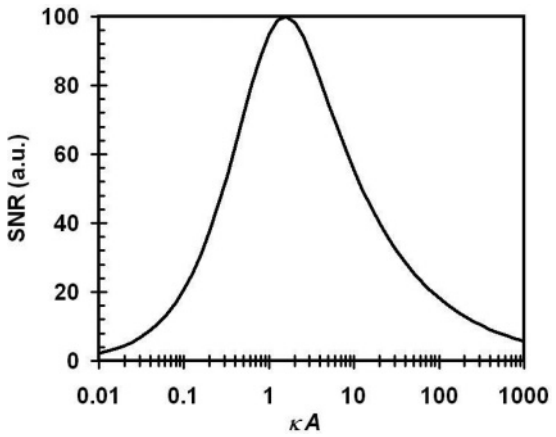

FIG. 5. Signal-to-noise ratio (SNR) as a function of the product between decay constant κ and amplitude A, where the decay constant κ is inverse to the interaction length λ, thus $\kappa = 1/\lambda$. Optimal SNR is obtained for $\kappa A = A/\lambda = 1.545$.

B. Frequency shift for a tip-sample force modeled by a Morse potential

We can now calculate the frequency shift assuming that a single chemical bond is responsible for the contrast. A covalent bond between a Si tip atom and an adatom on Si(111)-(7×7) can be modeled by a Morse potential,

$$V_{\mathrm{Morse}} = E_{\mathrm{bond}}(-2e^{-\kappa(z-\sigma)} + e^{-2\kappa(z-\sigma)}) \tag{32}$$

with the following fitting parameters: bond strength $E_{\mathrm{bond}} = 2.273$ eV, equilibrium distance $\sigma = 235.7$ pm, and decay constant $\kappa = 2 \times 1.497/0.2357\ \mathrm{nm}^{-1} = 12.70\ \mathrm{nm}^{-1}$.[36] The optimal amplitude to measure this bond in the attractive regime is therefore $A_{\mathrm{opt}} = 1.545/12.7$ nm = 122 pm. The repulsive regime of this bond would ideally be probed with an amplitude of 61 pm, because the range of the repulsive force component is only half the range of the attractive component. Figure 6 displays the force gradient and the frequency shifts corresponding to a sensor that oscillates in a force field given by this Morse potential.

Figure 6 shows that at the optimal oscillation amplitude, a minimal frequency shift of −70 Hz can be expected for a standard qPlus sensor and −3.5 Hz for a standard needle sensor when probing a single silicon bond. However, on weekly bonding systems such as organic molecules, absolute frequency shifts on the order of −5 Hz (Ref. 24) for a qPlus sensor with a contrast on the order of 0.1 Hz result. A needle sensor would change its frequency by only 0.25 Hz with a contrast of about 3 mHz for the same interaction.

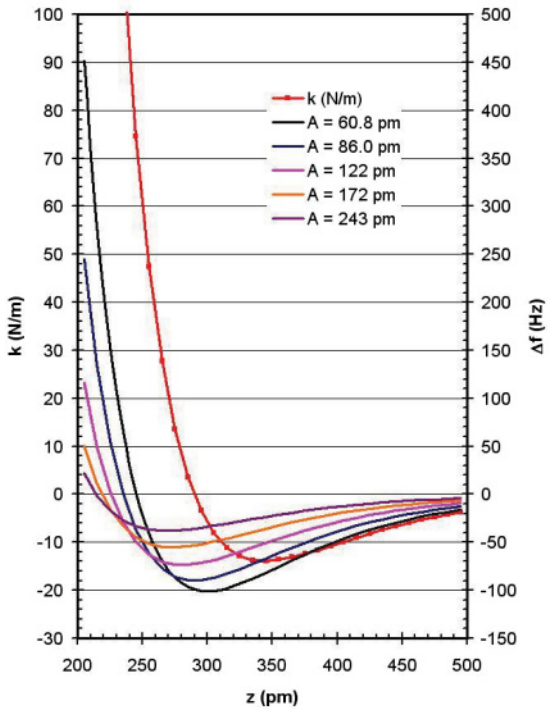

FIG. 6. (Color online) Force gradient (red) and calculated frequency shift for the interaction of a silicon tip with an adatom on the Si(111)-(7×7) surface modeled by a Morse potential with $E_{\text{bond}} = 2.273$ eV, $\sigma = 235.7$ pm, and $\kappa = 12.70$ nm^{-1} for a qPlus sensor with $k = 1800$ N/m and $f_0 = 30$ kHz and various amplitudes (see legend). If a standard needle sensor was used here, the frequency shift values denoted on the right vertical axis would have to be multiplied by 1/20, because the frequency shift is proportional to f_0/k. For the qPlus sensor, a minimal frequency shift of −70 Hz results at the optimal amplitude $A = 122$ pm, while the needle sensor only yields a minimal frequency shift of −3.5 Hz.

V. NOISE

If the frequency of the force sensor could be measured with infinite accuracy, infinitely small force gradients could be measured. In practice, there are four relevant noise contributions that need to be considered. For large bandwidths, i.e., for high scanning speeds, deflection detector noise is dominant. Deflection detector noise increases with $B^{3/2}$. Two other noise sources—thermal noise and oscillator noise—increase with the square root of bandwidth B. The fourth noise source is due to sensor frequency drifts caused by temperature changes. Thermal frequency drift is a challenge for room-temperature measurements and in particular for high-temperature measurements. Because we measure an average force gradient in FM-AFM, the noise in this figure is given with Eq. (2),

$$\delta k_{\text{ts}} = 2k\frac{\delta f}{f_0}. \tag{33}$$

A. Deflection detector noise

The deflection of the cantilever cannot be measured with infinite precision, but is subject to noise. Typically, the oscillation frequency of the cantilever varies very little around the eigenfrequency f_0 and we can therefore assume a constant deflection detector noise density n_q that denotes the precision at which the deflection of the cantilever can be measured (e.g., for $n_q = 100$ fm/$\sqrt{\text{Hz}}$, the error in deflection measurement is $\delta q = 100$ fm at a bandwidth of 1 Hz and $\delta q = 1$ pm at a bandwidth of 100 Hz). This uncertainty in the deflection measurement also leads to frequency noise,[37–39] given by

$$\frac{\delta f_{\text{det}}}{f_0} = \sqrt{\frac{2}{3}}\frac{n_q B^{3/2}}{A f_0}. \tag{34}$$

With Eq. (33), we find

$$\delta k_{\text{ts det}} = \sqrt{\frac{8}{3}}\frac{k n_q}{f_0}\frac{B^{3/2}}{A}. \tag{35}$$

For quartz sensors the deflection noise depends on the charge that is generated per deflection and the gain and noise of the preamplifier (see Fig. 7). Current-to-voltage converters convert the current provided by the quartz sensor to a voltage. However, the frequency response of the current-to-voltage converter is not independent of frequency, but is given by

$$V_{\text{out}} = -\frac{RI}{1 + i2\pi f RC}, \tag{36}$$

where R is the resistance of the feedback resistor and C is its parasitic capacitance. The red line in Fig. 8 shows the theoretical frequency response of an ideal operational amplifier with $R = 100$ MΩ and a parasitic capacitance of $C = 0.2$ pF. The gain is flat for frequencies smaller than the corner frequency $f_{c1} = 1/(2\pi RC) = 7.96$ kHz. For $f \gg f_{c1}$, the gain is given by $V_{\text{out}} = -I/(i2\pi f C)$—inversely proportional to f. A sinusoidally varying charge $Q_{\text{ch}} = Q_0 \exp(i2\pi f t)$ corresponds to a current $I = \dot{Q}_{\text{ch}} = Q_0 i2\pi f \exp(i2\pi f t)$, thus the gain can be expressed as $V_{\text{out}} = -Q_{\text{ch}}/C$. Therefore, this amplifier is called a "charge amplifier" for frequencies significantly larger than f_{c1}. Simple amplifiers such as the one shown in Fig. 7 often display a second corner frequency f_{c2} not very much higher than f_{c1}, and for frequencies beyond f_{c2} the gain decays proportional to $1/f^2$. The charge amplifier

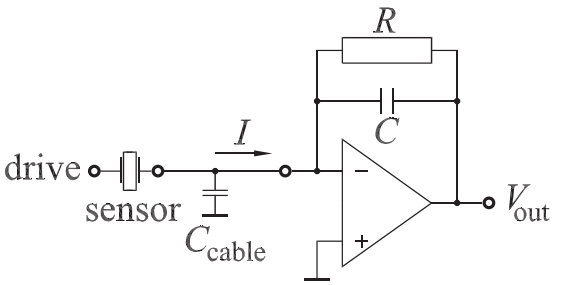

FIG. 7. Schematic of a quartz sensor, cable, and current-to-voltage converter that is often used for amplifying deflection data from quartz sensors. The gain of the amplifier is given by $V_{\text{out}} = -RI/(1 + if/f_{c1})$ with its first corner frequency f_{c1} given by $f_{c1} = 1/(2\pi RC)$. The capacity of the cable should be as low as possible—cable capacity increases noise in the amplifier output. If the amplifier is vacuum-compatible, it can be placed close to the sensor, thus reducing cable capacity and noise. The sensor can be excited electrically, as shown in this figure, or mechanically—the drive signal is grounded in this case.

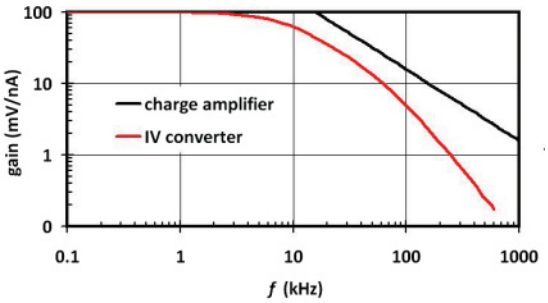

FIG. 8. (Color online) Current gain vs frequency for a current-to-voltage converter built from an ideal operational amplifier and a 100 MΩ feedback resistor with a parasitic capacitance of 0.2 pF (red line), yielding a first corner frequency (here, $f_{c1} = 8$ kHz). For frequencies higher than f_{c1}, the gain drops proportional to $1/f$. Typically, these simple amplifiers develop a second corner frequency (here $f_{c2} = 80$ kHz);[40] for frequencies higher than f_{c2}, their gain drops proportional to $1/f^2$. The black line displays the gain of a commercial charge amplifier[41] with a constant gain of 10^{13} V/C (black line) for a remarkably large frequency range from 250 Hz to 15 MHz.

that is used here for the needle sensor (Kolibri amplifier[41,49]) has an f_{c2} at around 15 MHz and is therefore suited well for high-frequency sensors. The question now is, when is it advisable to use a current-to-voltage converter, and when is it favorable to use a charge amplifier? Figure 8 shows that the current-to-voltage converter becomes a charge amplifier for sufficiently large frequencies. While one can increase f_{c1} by reducing the value of the feedback resistor R, a reduction of R increases the current noise. The tradeoff between noise and bandwidth leads to an optimal amplifier type for a given operating frequency. Here, we found that our home-built current-to-voltage converter has a better signal-to-noise ratio for frequencies around (30 ± 10) kHz, while the FEMTO amplifier[41] works better for higher frequencies. For charge amplifiers, the deflection detector noise density can be expressed by

$$n_q = \frac{n_{\mathrm{amp}}}{S}, \tag{37}$$

where n_{amp} is the noise density of the preamplifier and S is the sensitivity (charge per deflection) as calculated for the needle sensor in Eq. (28) and for the qPlus sensor in Eq. (19),

$$\delta k_{\mathrm{ts\,det}} = \sqrt{\frac{8}{3}} \frac{k}{S f_0} n_{\mathrm{amp}} \frac{B^{3/2}}{A}. \tag{38}$$

This equation shows that the deflection detector noise is small for small spring constants, small amplifier noise, large sensitivity, and large eigenfrequency. Thus, the figure of merit for the sensor is not S alone, but Sf_0/k. For both needle and qPlus sensors, the sensitivity is proportional to k. We find for the needle sensor

$$\delta k_{\mathrm{ts\,det\,ns}} = \sqrt{\frac{8}{3}} \frac{n_{\mathrm{amp}} t B^{3/2}}{d_{21} L A f_0} \tag{39}$$

for the ideal case of $L_e = L$. For the qPlus sensor, we find

$$\delta k_{\mathrm{ts\,det\,qPlus}} = \sqrt{\frac{8}{3}} \frac{n_{\mathrm{amp}} t^2 B^{3/2}}{6 d_{21} L^2 A f_0}, \tag{40}$$

again assuming the ideal case of $L_e = L$. Thus, deflection detector noise depends on the properties of the sensor and the amplifier. If we assume a charge noise density of $n_{\mathrm{amp}} = 90$ zC/$\sqrt{\mathrm{Hz}}$ (such as achieved by the commercial FEMTO amplifier[41] when loaded with a 1 m coaxial cable corresponding to a 100 pF cable capacitance), we can now calculate an explicit number for the deflection detector noise contribution to the force gradient noise with $A = 100$ pm and the geometrical values after Table I. For the needle sensor, we find a theoretical deflection detector noise contribution of

$$\delta k_{\mathrm{ts\,needle\,sensor}} = 33.2\ \mu\mathrm{N/m} \frac{B^{3/2}}{\mathrm{Hz}^{3/2}}, \tag{41}$$

and for the qPlus sensor, we find a theoretical deflection detector noise contribution of

$$\delta k_{\mathrm{ts\,qPlus\,sensor}} = 25.7\ \mu\mathrm{N/m} \frac{B^{3/2}}{\mathrm{Hz}^{3/2}}. \tag{42}$$

For a bandwidth of 100 Hz, the theoretical deflection detector noise contribution is thus 33.2 mN/m for the needle sensor and 25.7 mN/m for the qPlus sensor. However, we have based this calculation on the theoretical sensitivity of the sensors. We will see further below that while the experimental sensitivity of the needle sensor matches theory, the qPlus sensor develops only about 50% of the theoretical sensitivity. Deflection detector noise depends dramatically on bandwidth; it can be reduced substantially by bandwidth reduction. At low temperatures, where slow scanning is possible, the bandwidth can be reduced to 1 Hz or less and tiny force gradients can be detected in this case. For a bandwidth of 1 Hz, the deflection detector noise contribution is thus 33.2 μN/m for the needle sensor and 25.7 μN/m for the qPlus sensor. However, at low bandwidth the remaining three noise sources are typically much larger than the deflection detector noise.

B. Thermal noise

The thermal noise of a force sensor at a bandwidth B is given by[2]

$$\frac{\delta f_{\mathrm{thermal}}}{f_0} = \sqrt{\frac{k_B T B}{\pi k A^2 f_0 Q}}. \tag{43}$$

Thus, the thermal noise in force gradient measurement is given by

$$\delta k_{\mathrm{ts\,thermal}} = \sqrt{\frac{4 k k_B T B}{\pi A^2 f_0 Q}} \propto \sqrt{\frac{k}{f_0 Q}}. \tag{44}$$

For the needle sensor, reasonable Q values are 15 000 at room temperature and 80 000 at 4 K.[30] For the qPlus sensor, $Q \approx 3000$ at room temperature, reaching up to 200 000 at 4 K.[42] Thus, at room temperature the thermal contribution to the minimal detectable force gradient is $\delta k_{\mathrm{ts\,thermal}} = 6$ mN/m per $\sqrt{\mathrm{Hz}}$ for the needle sensor and $\delta k_{\mathrm{ts\,thermal}} = 3$ mN/m per $\sqrt{\mathrm{Hz}}$ for the qPlus sensor. At $T = 4$ K, the minimal detectable force gradient is $\delta k_{\mathrm{ts\,thermal}} = 390$ μN/m per $\sqrt{\mathrm{Hz}}$ for the needle sensor and $\delta k_{\mathrm{ts\,thermal}} = 40$ μN/m per $\sqrt{\mathrm{Hz}}$ for the qPlus sensor. Again, these calculations refer to $A = 100$ pm.

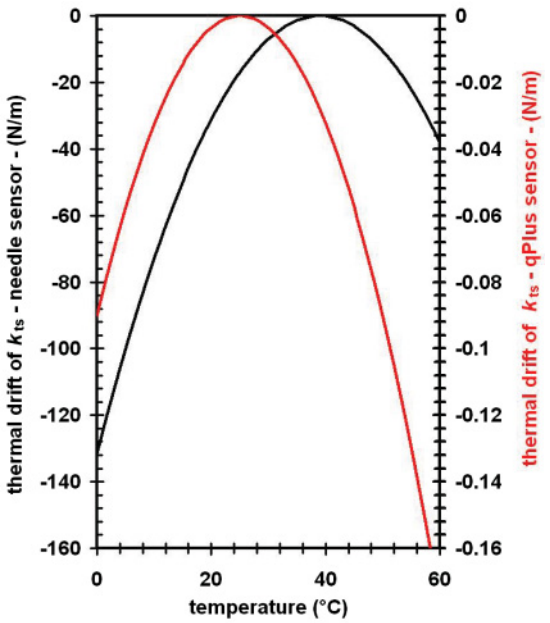

FIG. 9. (Color online) Effect of temperature changes on the measured tip-sample force gradient. Both the needle sensor and the qPlus sensor change their frequency as a function of temperature. Although the relative frequency shift is much smaller than for silicon cantilevers, the effect on the measured force gradient scales with stiffness k. This thermal frequency drift noise is almost three orders of magnitude smaller for the qPlus sensor than for the needle sensor.

C. Oscillator noise

Recently, Kobayashi *et al.*[39] discovered a new contribution to frequency noise in FM-AFM that arises in particular in low-Q environments. However, this contribution is not explicitly temperature-dependent and thus can become significant at low temperatures where thermal noise becomes small. The origin of this noise can be understood as a driving of the cantilever off resonance because the amplitude feedback is fed with a noisy input signal (due to a finite n_q). The lower the Q value, the more of this noise pushes the cantilever at the correct phase, therefore this noise contribution is proportional to n_q and inversely proportional to Q:

$$\frac{\delta f_{\rm osc}}{f_0} = \frac{n_q B^{1/2}}{\sqrt{2} A Q}. \tag{45}$$

With Eq. (33), we find

$$\delta k_{\rm ts\,osc} = \sqrt{2}\frac{k n_q}{Q}\frac{B^{1/2}}{A}. \tag{46}$$

Similar to thermal noise, oscillator noise is proportional to the square root of the detection bandwidth B and inversely proportional to amplitude. For the Q values given above, we find room-temperature values of $\delta k_{\rm ts\,osc} = 4.6$ mN/m per $\sqrt{\rm Hz}$ for the needle sensor and $\delta k_{\rm ts\,thermal} = 0.6$ mN/m per $\sqrt{\rm Hz}$ for the qPlus sensor. At $T = 4$ K, the contribution of oscillator noise to the minimal detectable force gradient is $\delta k_{\rm ts\,osc} = 1.4$ mN/m per $\sqrt{\rm Hz}$ for the needle sensor and $\delta k_{\rm ts\,thermal} = 9.5$ μN/m per $\sqrt{\rm Hz}$ for the qPlus sensor. Again, these calculations refer to $A = 100$ pm.

D. Thermal frequency drift noise

Temperature variations cause a drift in eigenfrequency. For silicon cantilevers, the relative frequency variation is linear with temperature with a value of -35 ppm/K at room temperature.[9] Thus, a hypothetical Si cantilever with $k = 1$ kN/m (this large stiffness would be required to enable stable oscillation at small amplitudes) would be subject to a $\langle k_{\rm ts}\rangle$ drift of -35 mN/m/ K. Quartz sensors show a quadratic frequency shift with temperature, and the eigenfrequency varies with temperature as an inverted parabola centered around the *turnover temperature* T_p,[43]

$$\frac{\delta f_{\rm sensor}}{f_0} = -\chi(T - T_p)^2. \tag{47}$$

The turnover temperature depends on the crystal cut (see Fig. 9 in Ref. 44). Tuning fork crystals are often cut to yield $T_p = 298$ K such that the turnover temperature is close to the temperature that a watch strapped to a wrist typically develops. Length-extensional resonators, in contrast, are often oriented such that their turnover temperature is around 313 K,[43] probably because 1 MHz crystals are typically not worn on the wrist but built into printed circuit boards that have higher operating temperatures than the human body. Here we chose an LER with $T_p = 298$ K to be able to compare the frequency drift of both types of sensors at room temperature. This thermal frequency drift causes a thermal drift in force gradient measurement given by

$$\delta k_{\rm ts\,drift} = -2k\chi(T - T_p)^2. \tag{48}$$

Although the temperature stability of quartz is excellent with very small values of $\chi = 35 \times 10^{-9}$ K^{-2},[43] the net effect on the precision on the measurement of $\langle k_{\rm ts}\rangle$ is proportional to the effective stiffness of the sensor k (see Fig. 9).

The quadratic dependence of the frequency variation with temperature is only valid for temperatures around T_p. For the temperature range from 300 to 4 K, the frequency variation has been measured by Hembacher *et al.*[45] and is approximately given by

$$\frac{\delta f_{\rm sensor}}{f_0} \approx -0.000\,81\{1 - \cos[(T/T_p - 1)\pi]\} \tag{49}$$

with a total relative frequency change of -1620 ppm over the temperature range from 300 to 4 K. An *et al.* have found a similar frequency change of a needle sensor (Fig. 3 in Ref. 30) from 998 066 Hz at 300 K to 996 314 Hz, corresponding to -1755 ppm. This equation shows that frequency drift with temperature is particularly large for temperatures between room temperature and absolute zero. This approximate formula models the data measured by Hembacher *et al.*[45] quite precisely down to liquid-helium temperatures. Because the relative frequency shift is mainly dependent on the variation of the velocity of sound with temperature (pp. 38 in Ref. 46), we expect a similar relative frequency shift for the qPlus sensor and the needle sensor also in the whole temperature range from 0 to 300 K.We now analyze the effect of temperature drift on the measured tip-sample force gradient. First, we look at the frequency drift of the sensor for a given rate of temperature change. Figure 10(a) shows temperature versus time for a constant drift rate of $dT/dt = 125$ μK/s at $T - T_p = 10$ K over a time interval of 10 min. The frequencies of quartz sensors

vary according to Eq. (47) by a rate $r_{\rm ns} = 100\ \mu$Hz/s for the needle sensor and $r_{\rm qPlus} = 3.3\ \mu$Hz/s for the qPlus sensor.

Now, we can compute the power spectral density of the frequency drift noise contribution by taking a Fourier transform of the square of the frequency drift. The reason we are not just adding the frequency noise contributions but adding the squares is that the detector, thermal oscillator, and thermal drift noise are statistically independent and the net effect of statistically independent variables is computed by taking the square root of the sum of squares. For a frequency drift that is linear with time, we find $\delta f(t) = r \times t$ within a time interval $[-\tau/2 \ldots \tau/2]$. With $\Omega = 2\pi/\tau$, we can express the time dependence of the frequency as

$$\delta f^2(t) = \sum_{n=0}^{\infty} a_n \cos(n\Omega t) \tag{50}$$

with Fourier coefficients

$$a_n = \frac{\Omega}{\pi} \int_{t=-\tau/2}^{\tau/2} r^2 t^2 \cos(n\Omega t) dt \tag{51}$$

and

$$a_n = (-1)^n \frac{r^2 \tau^2}{\pi^2 n^2}. \tag{52}$$

We can now interpret $|a_n|$ as the equivalent power component at a frequency $f_{\rm mod} = n/\tau$ in a frequency interval of $1/\tau$. Therefore, the power spectral density (power per frequency) becomes

$$n^2_{\Delta f\ \rm drift}(f_{\rm mod}) = \frac{r^2 \tau}{\pi^2 f^2_{\rm mod}} \tag{53}$$

and

$$n_{\Delta f\ \rm drift}(f_{\rm mod}) = \frac{r\sqrt{\tau}}{\pi f_{\rm mod}}. \tag{54}$$

Thus, a linear frequency drift leads to $1/f$ noise in the frequency spectrum of the phase-locked loop (PLL) output. The magnitude of this noise component depends on the drift rate of the frequency r and the measurement period τ. The time period τ is at least the time it takes to complete one image. Thus, for fast measurements, frequency drift noise can be reduced provided that the frequency detector (PLL) is reset before an image is taken. To obtain the effect of this noise on the force gradient measurement, we need to multiply $n_{\Delta f}(f_{\rm mod})$ by $2k/f_0$ [see Eq. (2)] to obtain

$$n_{k_{\rm ts}\ \rm drift}(f_{\rm mod}) = \frac{2kr\sqrt{\tau}}{f_0 \pi f_{\rm mod}}. \tag{55}$$

Because the frequency drift rate is proportional to f_0, the force gradient noise due to thermal drift is proportional to the stiffness of the sensor k, and thus this noise source is 600 times larger for the needle sensor than for the qPlus sensor. We also note, that there are other long-term frequency drift contributions that are difficult to quantify such as crystal aging etc. The effect of these frequency instabilites on the measurement of experimental force gradients are proportional to the stiffness of the sensors, and therefore these noise contributions are 600 times larger in the needle sensor than in the qPlus sensor.

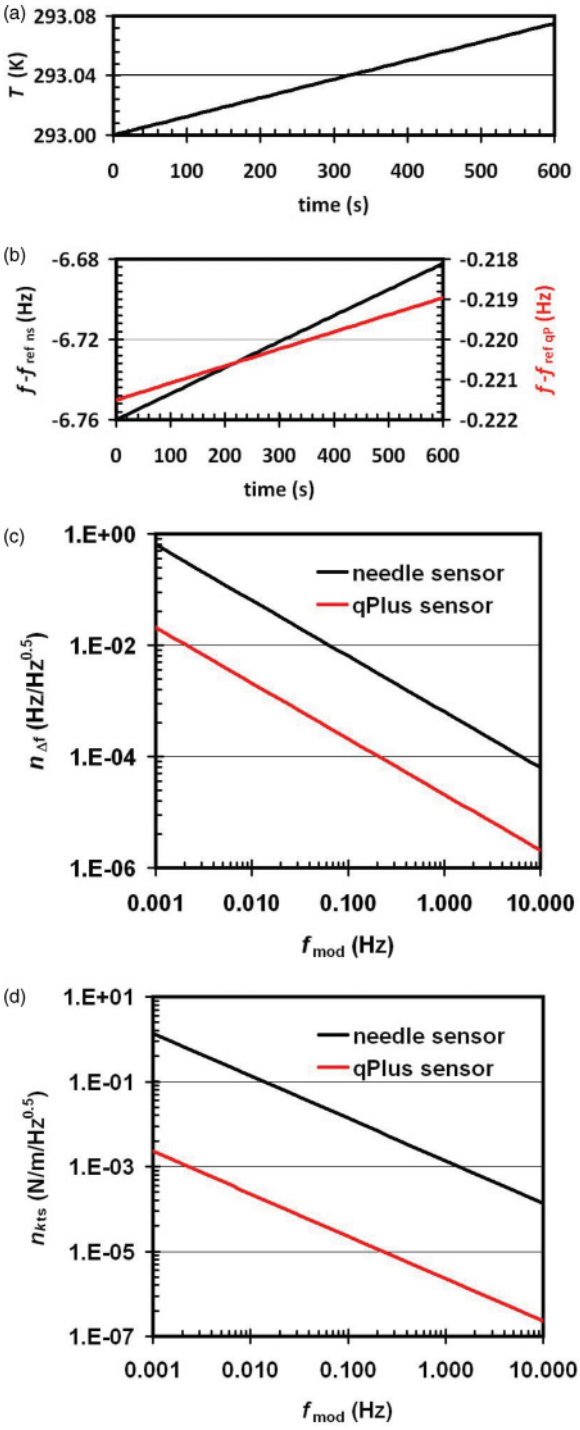

FIG. 10. (Color online) Effect of temperature drift on frequency drift, frequency noise at the PLL output, and force gradient noise. (a) A temperature drift of 125 μK/s is assumed, yielding a temperature increase of 75 mK over 10 min. (b) Frequency drift at at temperature 10 K above or below the turnover temperature T_p; see Eq. (47). For the needle sensor, the absolute frequency change over 10 min is 78 mHz, while for the qPlus sensor it is 2.5 mHz. (c) Power spectral density of the frequency drift noise for the needle and the qPlus sensors. A linear frequency drift with time causes a $1/f$ power spectrum. (d) Power spectral density of the tip-sample force gradient noise due to drift. This noise contribution is linear with the force constant of the sensor, i.e., it is 600 times larger for the needle sensor than for the qPlus sensor.

E. Summary of noise calculations

In summary, we find that the large spring constant of the needle sensor is not a significant disadvantage regarding deflection detector noise, because although the frequency shift that a sensor is subject to is proportional to $1/k$, the sensitivity is proportional to k, and the two effects cancel. However, k does affect the other three noise sources: thermal noise increases as $\sqrt{k}$, and both oscillator noise and frequency drift noise are proportional to k. Therefore, the recommendations in Eq. (1), stating that k should be large enough to enable stable sensor oscillations at the optimal amplitude but otherwise be as small as possible, are still valid. High-Q values are desirable to minimize thermal and oscillator noise. The frequency drift noise can be minimized by operating the sensors in a thermally stable environment, preferentially at temperatures at or close to T_p.

VI. EXPERIMENTAL NOISE MEASUREMENTS

A. Deflection spectrum at thermal excitation

So far, we have only considered theoretical calculations to compare the noise characteristics of the two sensors studied here. Now, we supplement the calculations by measurements. First, we measure the thermal noise peak of the needle sensor and the qPlus sensor with sensors of standard dimensions listed in Table I. The equipartition theorem states that an oscillator carries a thermal energy $k_BT/2$ per degree of freedom, where k_B is Boltzmann's constant and T is the temperature in degrees Kelvin. For the standard qPlus sensor, we find the thermal amplitude by equating the average potential energy to the thermal energy $kA_{\mathrm{rms}}^2/2 = k_BT/2$, yielding a thermal rms amplitude of $A_{\mathrm{rms}} = 1.52$ pm or a peak amplitude of $A_{0p} = 2.14$ pm. For the needle sensor, we need to take into account that it is a coupled oscillator, therefore $2 \times k'A_{\mathrm{rms}}^2/2 = k_BT/2$, yielding a thermal rms amplitude of $A_{\mathrm{rms}} = 62$ fm or a peak amplitude of $A_{0p} = 88$ fm. Figure 11 shows the thermal peak of a needle sensor without tip in ambient conditions. The power spectral density in Fig. 11 was recorded by connecting the output of the FEMTO amplifier[41] to the input of the oscillation controller (OC4 from Nanonis[47]) using the Zoom-FFT (fast Fourier transform) feature and correcting the filter error by comparing the output with a dedicated FFT analyzer at low frequencies (Agilent 35670A Dynamical Analyzer). The input of the FEMTO amplifier was connected to a length extensional resonator (no tip attached) with dimensions given by Table I with a coaxial cable with a length of 1 m (capacity approximately 100 pF). The commercial preamplifier has a noise density of $n_{\mathrm{amp}} = 90$ zC/$\sqrt{\mathrm{Hz}}$ when loaded with a 1 m coaxial cable (100 pF cable capacitance)[41] and $n_{\mathrm{amp}} = 40$ zC/$\sqrt{\mathrm{Hz}}$ without a cable (sensor directly connected to the amplifier) at the operating frequency of the needle sensor (1 MHz). From Fig. 11, we can calculate the sensitivity as well as the deflection detector noise density by following the procedure published in Ref. 16.

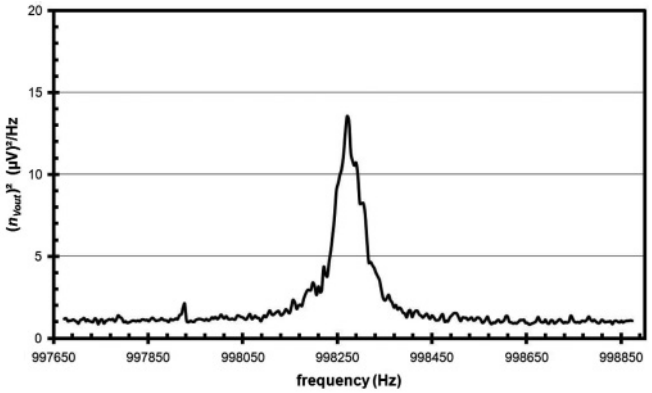

FIG. 11. Thermal spectrum of a needle sensor with standard dimensions at room temperature and ambient pressure. A commercial preamplifier[41] was used. The sensitivity of the sensor is calculated to 45.4 μC/m, the Q factor is 18 500, and the deflection detector noise density is 1.89 fm/$\sqrt{\mathrm{Hz}}$. The Q-factor is determined by fitting the resonance curve of a damped harmonic oscillator to the thermal spectrum.

For the needle sensor, we find an experimental sensitivity of $S_{\mathrm{needle\ sensor}}^{\mathrm{exp}} = 45.4\ \mu$C/m, which is 100% of the theoretical value. In a previous measurement, the needle sensor reached only 44% of the theoretical value.[29] A possible reason for a deviation between theoretical and experimental sensitivity in the previous measurement might be attributed to cable capacity between sensor and amplifier and nonideal amplifier performance. The deflection detector noise density is thus $n_q = 2$ fm/$\sqrt{\mathrm{Hz}}$ with a 1 m cable and $n_q = 0.89$ fm/$\sqrt{\mathrm{Hz}}$ when the sensor is directly connected to the preamp (not feasible for vacuum operation).

At 30 kHz, the operating frequency of the qPlus sensor, we measured $n_{\mathrm{amp}} = 122$ zC/$\sqrt{\mathrm{Hz}}$ with a 1 m coaxial cable (100 pF cable capacitance) for the FEMTO amplifier[41] and $n_{\mathrm{amp}} = 86$ zC/$\sqrt{\mathrm{Hz}}$ without a cable. Thus, a standard qPlus sensor would yield $n_q = 122$ zC/$\sqrt{\mathrm{Hz}}$/1.44 μC/m = 85 fm/$\sqrt{\mathrm{Hz}}$. When directly connected to the commercial amplifier, the qPlus sensor would achieve a deflection detector noise density of $n_q = 60$ fm/$\sqrt{\mathrm{Hz}}$ at room temperature. Using our home-built amplifier for the qPlus sensor, we obtained a deflection detector noise density of $n_q = 62$ fm/$\sqrt{\mathrm{Hz}}$ (see Fig. 12). The home-built amplifier is a current-to-voltage converter based on an OPA 657 operational amplifier with

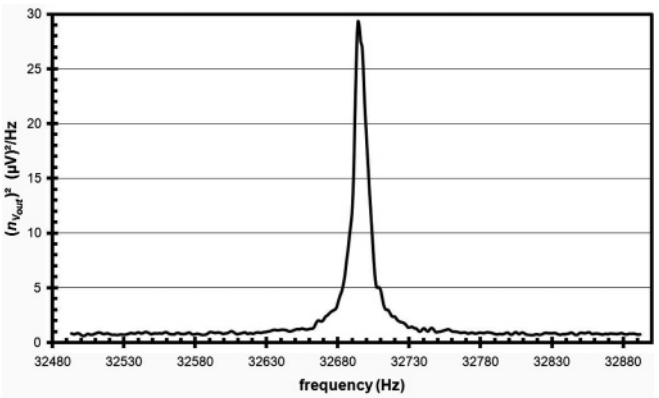

FIG. 12. Thermal spectrum of a qPlus sensor with standard dimensions at room temperature and ambient pressure. A home-built preamplifier was used. The sensitivity of the sensor is calculated to 1.44 μC/m, the Q factor is 2900, and the deflection detector noise density is 62 fm/$\sqrt{\mathrm{Hz}}$.

a feedback resistance of 100 MΩ.[17] The power spectral density in Fig. 12 was recorded by connecting the output of a home-built UHV-compatible amplifier to the input of a FFT analyzer (Agilent 35670A Dynamical Analyzer). This thermal noise spectrum allows to determine all the relevant noise data of the sensor and its amplifier as shown in Ref. 48. The input of the amplifier was connected to a qPlus sensor without tip with dimensions given by Table I with a short cable with a length of approximately 0.1 m (capacity approximately 1 pF). The experimental result is $S_{\mathrm{qPlus}}^{\mathrm{exp}} = 1.44\ \mu\mathrm{C/m}$—about 51% of the theoretical value. The deviation between the theoretical and experimental values is probably due to edge effects—the calculation of the sensitivity is based on a homogeneous field distribution and an electrode configuration in the quartz crystal as in Fig. 3(e), while the actual field distribution is perturbed by edge effects as in Fig. 3(c). For the needle sensor, the deviation between the actual [Fig. 3(h)] and the ideal field [Fig. 3(j)] is much smaller, therefore its experimental sensitivity is essentially equal to the calculated sensitivity. It is UHV-compatible and therefore can be connected closely to the sensor, thereby greatly reducing C_{cable}. At low temperatures the home-built amplifier can be cooled, and its noise at 4 K typically drops to 50%,[45] yielding $n_q = 31\ \mathrm{fm}/\sqrt{\mathrm{Hz}}$ at 4 K.

B. Power spectral density of the frequency detector output

When the sensor is operating in the AFM, it is excited at a constant amplitude, and the frequency of the sensor is measured as the physical observable that relates to the tip-sample forces.

Figure 13 shows the calculated (smooth lines) and experimental (jagged lines) power spectral density of the force gradient noise $n_{k_{\mathrm{ts}}}$ as a function of modulation frequency f_{mod}. This graph is produced by inserting the output of the phase-locked-loop detector to a FFT analyzer (Agilent) and multiplying the spectral frequency shift noise density

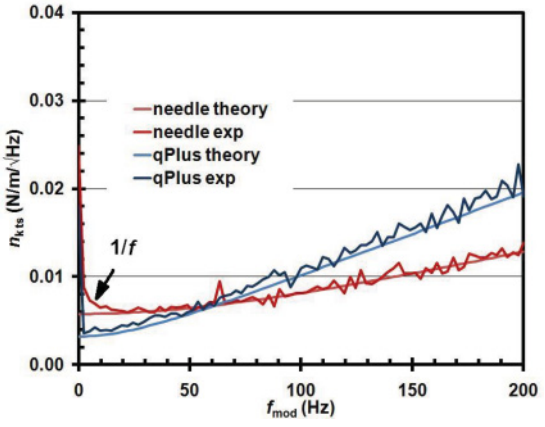

FIG. 13. (Color online) Total experimental and calculated force-gradient noise densities as a function of modulation frequency for the needle sensor (red line) and the qPlus sensor (blue line) at room temperature. The calculated force-gradient noise densities are derived with the experimental values for S, k, n_{amp}, Q, and f_0 at an amplitude of $A = 100$ pm. The $1/f$ component for small f_{mod} is due to thermal frequency drift noise [see Eq. (55)].

by the corresponding scaling factor ($k_{\mathrm{ts}} = 2k/f_0 \times \Delta f$, thus $n_{k_{\mathrm{ts}}} = 2k/f_0 \times n_{\Delta f}$). For these measurements, it is essential that the Nanonis OC4 PLL is set to sufficiently fast settings (here, demodulation bandwidth 1300 Hz, lock range 305 Hz).

All four noise sources contribute to the experimental noise graphs. The absolute force gradient noise figures outlined in Sec. V can be transformed in a density representation by

$$n_{k_{\mathrm{ts}}}(f_{\mathrm{mod}}) = \sqrt{\left.\frac{\partial \delta k_{\mathrm{ts}}^2}{\partial B}\right|_{B=f_{\mathrm{mod}}}}. \tag{56}$$

Thus, we can explicitly calculate the four spectral noise contributions from quantities that can be obtained from the thermal noise spectrum as shown in Fig. 12 and a measurement of sensor stiffness.

(i) For the detector noise contribution, we find

$$n_{k_{\mathrm{ts}}\,\mathrm{det}}(f_{\mathrm{mod}}) = \sqrt{8}\frac{k n_q}{f_0 A} f_{\mathrm{mod}}. \tag{57}$$

(ii) Thermal noise is constant with respect to f_{mod}:

$$n_{k_{\mathrm{ts}}\,\mathrm{th}} = \sqrt{\frac{4 k k_B T}{\pi A^2 f_0 Q}}. \tag{58}$$

(iii) Oscillator noise is also constant with f_{mod}:

$$n_{k_{\mathrm{ts}}\,\mathrm{osc}} = \sqrt{2}\frac{k n_q}{Q A}. \tag{59}$$

(iv) Frequency drift noise is inversely proportional to f_{mod}:

$$n_{k_{\mathrm{ts}}\,\mathrm{drift}}(f_{\mathrm{mod}}) = \frac{2kr\sqrt{\tau}}{f_0 \pi f_{\mathrm{mod}}}. \tag{60}$$

The total noise of the force gradient measurement is given by

$$\delta k_{\mathrm{ts}} = \sqrt{\int_{1/\tau}^{B} n_{k_{\mathrm{ts}}}^2(f_{\mathrm{mod}}) df_{\mathrm{mod}}} \tag{61}$$

with

$$n_{k_{\mathrm{ts}}}^2(f_{\mathrm{mod}}) = n_{k_{\mathrm{ts}}\,\mathrm{det}}^2(f_{\mathrm{mod}}) + n_{k_{\mathrm{ts}}\,\mathrm{th}}^2 + n_{k_{\mathrm{ts}}\,\mathrm{osc}}^2 + n_{k_{\mathrm{ts}}\,\mathrm{drift}}(f_{\mathrm{mod}})^2. \tag{62}$$

The calculated graphs include deflection detector noise (linear with f_{mod}), thermal noise (constant with f_{mod}), and oscillator noise (also constant with f_{mod}). Frequency drift noise, which is large for long measuring times (i.e., small f_{mod}), is not included in the calculation, but clearly apparent in the measurement by the increase of the experimental needle deflection detector noise density for small f_{mod}. As expected, the qPlus sensor shows less thermal, oscillator, and frequency drift noise, but more detector noise. This is due to the excellent adaption of the FEMTO/Kolibri amplifier[41,50] to the needle sensor, and to the fact that the standard qPlus sensor as described in Table I only has 50% of the calculated sensitivity.

Table II summarizes the results in a way that all noise contributions can be identified.

TABLE II. Noise contributions of the four noise sources for the qPlus sensor ($f_0 = 30$ kHz) and the needle sensor ($f_0 = 998$ kHz) for $A = 100$ pm and $B = 1$ Hz. Note that detector noise scales with $B^{3/2}$ [after Eq. (34)], while thermal noise [after Eq. (44)] and oscillator noise [after Eq. (46)] scale with $B^{1/2}$. Thus for $B = 100$ Hz, detector noise would increase by a factor of 1000, while thermal and oscillator noise would only increase by a factor of 10. Frequency drift noise [after Eq. (48)] is independent of amplitude and becomes large for small bandwidths. For both sensors, the $\delta k_{\mathrm{ts\,drift}}$ data at 300 K are based on the parabolic frequency drift according to Eq. (47) for $T = T_p \pm 2$ K, while the data at 4 K are based on a relative frequency drift of 1 ppm/K (see fig. 2 in Ref. 49).

Sensor	n_q ($\frac{\mathrm{fm}}{\mathrm{Hz}^{1/2}}$)	Q	$\frac{\delta k_{\mathrm{ts\,det}}}{B^{3/2}}$ ($\frac{\mu\mathrm{N/m}}{\mathrm{Hz}^{3/2}}$)	$\frac{\delta k_{\mathrm{ts\,th}}}{B^{1/2}}$ ($\frac{\mu\mathrm{N/m}}{\mathrm{Hz}^{1/2}}$)	$\frac{\delta k_{\mathrm{ts\,osc}}}{B^{1/2}}$ ($\frac{\mu\mathrm{N/m}}{\mathrm{Hz}^{1/2}}$)	$\delta k_{\mathrm{ts\,drift}}$ (300 K) ($\frac{\mathrm{mN}}{\mathrm{m}}$), $\Delta T = 0.1$ K	$\delta k_{\mathrm{ts\,drift}}$ (4 K) ($\frac{\mathrm{mN}}{\mathrm{m}}$), $\Delta T = 10$ mK
qPlus 300 K air	62	2900	60.7	3290	544	0.05	
qPlus 300 K UHV	62	5000	60.7	2510	316	0.05	
qPlus 4 K UHV	31	200 000	30.4	46	4		0.036
needle 300 K air	1.89	18 500	33.4	5530	1560	31	
needle 300 K UHV	1.89	50 000	33.4	3370	577	31	
needle 4 K UHV	1.89	80 000	33.4	308	361		21.6

VII. SUGGESTIONS FOR IMPROVEMENTS ON QPLUS AND LER SENSORS

A. Decreasing deflection detector noise

With the equations that link signal and noise to the physical parameters of the sensors, we can now attempt to tailor the design values for optimal performance. Equation (40) connects the relative frequency noise (detector contribution) to the sensitivity of the sensor and the noise performance of the amplifier. For both sensors, we find

$$\delta k_{\mathrm{ts\,det}} = 2k\sqrt{\frac{2}{3}}\frac{n_{\mathrm{amp}}}{SAf_0}B^{3/2}. \tag{63}$$

With Eqs. (20), (21), and (28) in the ideal situation of $L_e = L$, we can express the spring constant k, sensitivity S, and eigenfrequency f_0 in terms of the geometrical parameters t, w, and L, we find for the detector noise contribution for the needle sensor:

$$\delta k_{\mathrm{ts\,det\,ns}} = 8\sqrt{\frac{2}{3}}\frac{n_{\mathrm{amp}}t}{d_{21}Av_s}B^{3/2}. \tag{64}$$

For the qPlus sensor, we use Eqs. (17), (18), and (19) assuming again $L_e = L$, finding

$$\delta k_{\mathrm{ts\,det\,qPlus}} = 2.06\sqrt{\frac{2}{3}}\frac{n_{\mathrm{amp}}t}{d_{21}Av_s}B^{3/2}. \tag{65}$$

This result seems quite surprising: deflection detector noise only depends on the thickness t of the sensor—all the other geometrical dimensions cancel, and when comparing a qPlus and a needle sensor with the same thickness, the qPlus sensor should only display about 1/4 of the noise of the needle sensor if the charge noise of the amplifier in use is similar. If we take into account that the quartz-cantilever geometry only produces about 50% of the theoretical sensitivity, a qPlus sensor with the same thickness of a needle sensor should display only 1/2 of the noise. Miniaturization, therefore, appears to be the road to success. The reason for the superior signal-to-noise ratio of the cantilever geometry implemented in the qPlus sensor over the length-extensional principle utilized in the needle sensor lies in the fact that the cross section of the qPlus sensor beam shows a strain and stress profile that is zero in the center and increases toward the edges, where the charge-collecting electrodes are located, while the cross section of the needle sensor has a uniform stress and strain profile [see Figs. 3(d) and 3(h)]. Figure 14 displays the noise figures of standard needle and qPlus sensors and a modified qPlus sensor with a smaller thickness t and smaller length L with $f_0 = 92.8$ kHz, $k = 3500$ N/m, $Q = 1650$, and $n_q = 28\,\mathrm{fm}/\sqrt{\mathrm{Hz}}$. This sensor is not only superior to the needle sensor in thermal, oscillator, and frequency drift noise, but also in detector noise.

B. Decreasing thermal noise

As outlined in Eq. (44), the thermal noise in the force gradient measurement is given by

$$\delta k_{\mathrm{ts\ thermal}}(z) = \sqrt{\frac{4kk_BTB}{\pi A^2 f_0 Q}}. \tag{66}$$

Thus, thermal noise can be minimized by a reduction of temperature, using a stiffness k as small as possible compatible with stability and choosing a high eigenfrequency f_0 while maintaining a high-Q value.

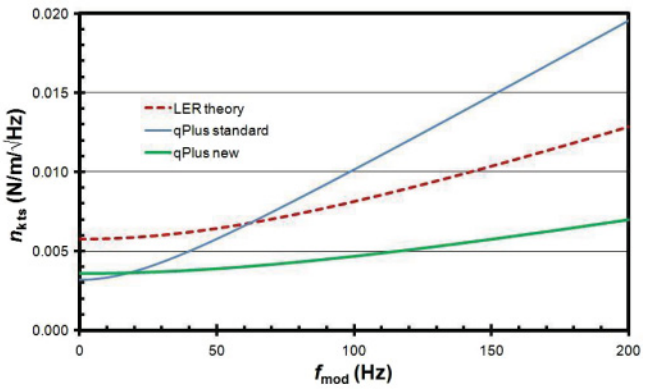

FIG. 14. (Color online) Calculated force-gradient noise densities $n_{k_{\mathrm{ts}}}$ as a function of modulation frequency for the standard needle sensor (red line), qPlus sensor (blue line), and a modified qPlus sensor with $f_0 = 92.8$ kHz, $k = 3500$ N/m, $Q = 1650$, and $n_q = 28\,\mathrm{fm}/\sqrt{\mathrm{Hz}}$ (green line). The calculated values for $n_{k_{\mathrm{ts}}}$ are based on measured values of n_{amp}, S, k, f_0, and Q.

C. Decreasing oscillator noise

Oscillator noise can be minimized by combining the recipes to reduce deflection detector noise and thermal noise, because oscillator noise goes down with decreasing deflection detector noise, increasing Q, and minimizing k.

D. Decreasing frequency drift noise

Again, frequency drift noise is minimized by choosing the appropriate stiffness k of the cantilever. Because frequency drift noise is proportional to k, we need a stiffness as small as possible (yet allowing stable oscillation at small amplitudes). A second factor concerns temperature stabilization and choosing an operating temperature close to the turnover temperature of the corresponding quartz crystal orientation. Another possibility would be to tailor the turnover temperature of the quartz crystal by cutting it along the corresponding crystal direction. For the needle sensor, it might be useful to trigger the frequency detector (PLL) with an atomic clock because the frequency shift changes can become very small for weakly interacting samples. More precise measurements on the thermal frequency variation at low temperatures are needed to assess frequency drift noise for cryogenic microscopes (here, we have used a value of 1 ppm/K according to Fig. 2 in Ref. 49).

VIII. PRACTICAL CONSIDERATIONS REGARDING TIP MOUNTING

Tip mass plays a crucial role in the needle sensor, because an imbalance in the effective mass of the coupled beams reduces Q. Rychen has analyzed the effect of mass imbalance and found that for tuning fork geometries, an imbalance of 1.5% leads to a drop of the Q value by 63.5% (Fig. 4.8 in Ref. 51). Probably, the effect of mass imbalance is smaller for length extensional resonators than for tuning forks, however mass imbalance will effect the Q value of the needle sensor. Therefore, the tip of a needle sensor needs to be very small. Long and thin tips, however, can show significant thermal lateral oscillations and bend strongly under lateral forces. Young's modulus of tungsten is around 400 GPa, thus a wire with a diameter of 0.01 mm and a length of 0.3 mm has a lateral stiffness of only 22 N/m. In contrast, the qPlus sensor can easily accommodate heavy and more stable tips that can be resharpened more easily, with significant abrasion[52] and even cleaved *in situ*.[53]

IX. NOISE COMPARISON BETWEEN LARGE-AMPLITUDE (Si CANTILEVERS) AND SMALL-AMPLITUDE (QUARTZ SENSORS) OPERATION

This paper focuses on quartz force sensors, but many impressive results have been obtained with AFM using Si cantilevers, such as high-resolution force spectroscopy[54] imaging the rest atoms on Si(111)-(7×7),[37,55] imaging of insulators,[56,57] atomic manipulation,[58] chemical identification,[59] and the detection of short-range magnetic exchange forces.[60] It is instructive to compare the noise performance of quartz sensors with silicon cantilevers. When comparing only the thermal force gradient noise for silicon cantilevers and quartz sensors (see Table I in Ref. 31), Si cantilevers appear to be superior by more than four orders of magnitude. However, we need to consider that Si cantilevers cannot be operated in the force gradient regime when the tip comes close enough to feel chemical bonding forces.[61,62] Standard Si cantilevers need to be operated at amplitudes of about 10 nanometers, and the frequency shift in that case is given by the normalized frequency shift γ (Ref. 61) with

$$\gamma = \frac{\Delta f}{f_0} k A^{3/2} \approx \frac{1}{\sqrt{2\pi}} F_{\mathrm{ts}} \lambda^{1/2}, \tag{67}$$

where F_{ts} is the tip-sample force and λ is its range.[33,61] For small-amplitude operation, we find

$$k_{\mathrm{ts}} = 2k \frac{\Delta f}{f_0}. \tag{68}$$

While we cannot compare a minimal detectable force gradient and a minimal detectable normalized frequency shift, we can calculate a minimal detectable force $\delta F_{\mathrm{ts\,min}}$ for a given range λ. For the large-amplitude regime, we find

$$\delta F_{\mathrm{ts\,min}} = \sqrt{2\pi} k \frac{\delta \Delta f_{\mathrm{min}}}{f_0} \frac{A^{3/2}}{\lambda^{1/2}}. \tag{69}$$

For small amplitudes, the force noise is given by the product between the minimal detectable force gradient and the range

$$\delta F_{\mathrm{ts\,min}} = 2k \frac{\delta \Delta f_{\mathrm{min}}}{f_0} \lambda. \tag{70}$$

As shown in Table III, Si cantilevers with refined optical readout schemes are better in detector, thermal, and oscillator noise but show profoundly larger thermal drift noise. Also shown are the calculated noise figures for a qPlus sensor with optical deflection detection, reaching lower values for

TABLE III. Noise contributions of the four noise sources for different Si cantilevers, the qPlus sensor, the needle sensor, and $B = 1$ Hz with respect to an exponential attractive force with $\lambda = 79$ pm (Morse potential, as shown in Fig. 6).

Sensor	k (N/m)	f_0 (kHz)	n_q ($\frac{\mathrm{fm}}{\mathrm{Hz}^{1/2}}$)	Q	A (nm)	$\frac{\delta F_{\mathrm{ts\,det}}}{B^{3/2}}$ ($\frac{\mathrm{fN}}{\mathrm{Hz}^{3/2}}$)	$\frac{\delta F_{\mathrm{ts\,th}}}{B^{1/2}}$ ($\frac{\mathrm{fN}}{\mathrm{Hz}^{1/2}}$)	$\frac{\delta F_{\mathrm{ts\,osc}}}{B^{1/2}}$ ($\frac{\mathrm{fN}}{\mathrm{Hz}^{1/2}}$)	$\delta F_{\mathrm{ts\,drift}}$ (300 K) (pN), $\Delta T = 0.1$ K
Si cantilever[37,63]	46	298.0	272	54200	4	0.6	34	2.9	11.5
Si cantilever[64]	42	281.5	17	50000	8	0.04	50	0.3	29.7
qPlus opt. det.[65]	1500	27.8	15	6100	0.1	1.0	170	4.1	0.003
qPlus el. det.	1800	32.8	62	2900	0.1	4.4	250	43	0.004
needle	1080000	1000	1.89	18500	0.1	2.6	437	123	2.5

detector noise than in the electrically detected mode.[65] At low temperatures, the first three noise types decrease significantly for quartz sensors, but it is unclear how effective a Si cantilever can be cooled even in a low-temperature environment when intense laser light from the optical deflection detector is shined on them. Although Si cantilevers with good optical deflection detectors show less noise than quartz cantilevers, detector noise, thermal noise, and oscillator noise can be reduced by bandwidth reduction, and the thermal drift noise is significantly smaller for quartz cantilevers than for Si cantilevers.

X. SUMMARY AND OUTLOOK

Concluding, we compared force sensors based on length-extensional resonators and based on quartz tuning forks. We found that in contrast to applications in the literature, the effective spring constant of a needle sensor is actually twice as large as the stiffness of one tine [see Eq. (16)]. We have discussed four types of noise: deflection detector noise, thermal noise, oscillator noise, and frequency drift noise. Surprisingly, the deflection detector noise is independent of sensor stiffness, because while a stiffer sensor has less frequency shift proportional to $1/k$, its deflection signal increases linear with k. The other three noise sources, however, clearly favor sensors with spring constants around 1 kN/m. The cantilever geometry provides more charge per force than the length-extensional geometry. However, the longitudinal outline of the needle sensor is more suited to a space-conserving microscope.

ACKNOWLEDGMENTS

We thank Federico de Faria-Elsner, Joachim Welker, and Jay Weymouth for writing the software that analyzes the thermal peak and deflection noise densities. We are grateful to Stefan Torbrügge, Gerhard Meyer, and Fabian Mohn for helpful comments.

*franz.giessibl@physik.uni-regensburg.de
†eggy@ncassembly.jst.go.jp

[1] G. Binnig, C. F. Quate, and Ch. Gerber, Phys. Rev. Lett. **56**, 930 (1986).
[2] T. R. Albrecht, P. Grutter, H. K. Horne, and D. Rugar, J. Appl. Phys. **69**, 668 (1991).
[3] M. Tortonese, R. C. Barrett, and C. F. Quate, Appl. Phys. Lett. **62**, 834 (1993).
[4] F. J. Giessibl, Science **267**, 68 (1995).
[5] F. J. Giessibl, Rev. Mod. Phys. **75**, 949 (2003).
[6] F. J. Giessibl, H. Bielefeldt, S. Hembacher, and J. Mannhart, Appl. Surf. Sci. **140**, 352 (1999).
[7] M. Schmid, J. Mannhart, and F. J. Giessibl, Phys. Rev. B **77**, 045402 (2008).
[8] G. Meyer and N. M. Amer, Appl. Phys. Lett. **53**, 1045 (1988).
[9] U. Gysin, S. Rast, P. Ruff, E. Meyer, D. W. Lee, P. Vettiger, and C. Gerber, Phys. Rev. B **69**, 045403 (2004).
[10] P. Güthner, U. Fischer, and K. Dransfeld, Appl. Phys. B **48**, 89 (1989).
[11] K. Dransfeld, P. Guethner, and K. Heitmann, US Patent 5, 212, 987, US Patent and Trademark Office (1993).
[12] K. Bartzke, T. Antrack, K.-H. Schmidt, E. Dammann, and C. H. Schatterny, Int. J. Optoelectron. **8**, 669 (1993).
[13] K. Bartzke, T. Antrack, K. Besocke, and E. Dammann, Patent DE-19513529A1, German Patent and Trademark Office (1995).
[14] F. J. Giessibl, Patent DE-19633546, German Patent and Trademark Office (1996).
[15] F. J. Giessibl, Appl. Phys. Lett. **73**, 3956 (1998).
[16] F. J. Giessibl, Appl. Phys. Lett. **76**, 1470 (2000).
[17] I. Morawski, J. Blicharski, B. Voigtländer, Rev. Sci. Instrum. **82**, 063701 (2011).
[18] F. J. Giessibl, S. Hembacher, H. Bielefeldt, and J. Mannhart, Science **289**, 422 (2000).
[19] S. Hembacher, F. J. Giessibl, and J. Mannhart, Science **305**, 380 (2004).
[20] F. J. Giessibl, M. Herz, and J. Mannhart, Proc. Natl. Acad. Sci. (USA) **99**, 12006 (2002).
[21] S. Hembacher, F. J. Giessibl, J. Mannhart, and C. F. Quate, Phys. Rev. Lett. **94**, 056101 (2005).
[22] M. Ternes, C. Lutz, C. F. Hirjibehedin, F. J. Giessibl, and A. Heinrich, Science **319**, 1066 (2008).
[23] L. Gross, F. Mohn, P. Liljeroth, J. Repp, F. J. Giessibl, and G. Meyer, Science **324**, 1428 (2009).
[24] L. Gross, F. Mohn, N. Moll, P. Liljeroth, and G. Meyer, Science **325**, 1110 (2009).
[25] L. Gross, F. Mohn, N. Moll, G. Meyer, R. Ebel, W. M. Abdel-Mageed, and M. Jaspars, Nat. Chem. **2**, 821 (2010).
[26] M. Ternes, C. Gonzalez, C. P. Lutz, P. Hapala, F. J. Giessibl, P. Jelinek, and A. J. Heinrich, Phys. Rev. Lett. **106**, 016802 (2011).
[27] Z. Sun, M. P. Boneschanscher, I. Swart, D. Vanmaekelbergh, and P. Liljeroth, Phys. Rev. Lett. **106**, 046104 (2011).
[28] A. J. Weymouth, T. Wutscher, J. Welker, T. Hofmann, and F. J. Giessibl, Phys. Rev. Lett. **106**, 226801 (2011).
[29] T. An, T. Eguchi, K. Akiyama, and Y. Hasegawa, Appl. Phys. Lett. **87**, 133114 (2005).
[30] T. An, T. Nishio, T. Eguchi, M. Ono, A. Nomura, K. Akiyama, and Y. Hasegawa, Rev. Sci. Instrum. **79**, 033703 (2008).
[31] S. Torbrügge, O. Schaff, and J. Rychen, J. Vac. Sci. Technol. B **28**, C4E12 (2010).
[32] F. J. Giessibl, Appl. Phys. Lett. **78**, 123 (2001).
[33] F. J. Giessibl and H. Bielefeldt, Phys. Rev. B **61**, 9968 (2000).
[34] C. J. Chen, *Introduction to Scanning Tunneling Microscopy* (Oxford University Press, New York, 1993).
[35] R. W. Ward, *Constants of Alpha Quartz*, in *Piezoelectricity*, edited by C. Zwick Rosen, B. V. Hiremath, and R. Newnham(American Institute of Physics, New York, 1992), pp. 211–220.
[36] R. Perez, I. Stich, M. C. Payne, and K. Terakura, Phys. Rev. B **58**, 10835 (1998).
[37] T. Eguchi and Y. Hasegawa, Phys. Rev. Lett. **89**, 266105 (2002).
[38] Y. Hasegawa, T. Eguchi, T. An, M. Ono, K. Akiyama, and T. Sakurai, Jpn. J. Appl. Phys. **43**, L303 (2004).

[39]K. Kobayashi, H. Yamada, and K. Matsushige, Rev. Sci. Instrum. **80**, 043708 (2009).
[40]F. de Faria Elsner, Diploma thesis in experimental physics, University of Regensburg, Germany, 2010.
[41]Femto HQA-15M-10T, Femto GmbH, Berlin, Germany.
[42]T. Hofmann, J. Welker, and F. J. Giessibl (unpublished).
[43]Microcrystal product brochure, Micro Crystal AG, Mühlestrasse 14, CH-2540 Grenchen, Switzerland.
[44]E. Momosaki and Sh. Kogure, in *Piezoelectricity*, edited by G. W. Taylor, J. J. Gagnepain, T. R. Meeker, T. Nakamura, and L. A. Shuvalov (Gordon and Breach, New York, 1985), pp. 47–60.
[45]S. Hembacher, F. J. Giessibl, and J. Mannhart, Appl. Surf. Sci. **188**, 445 (2002).
[46]*Noncontact Atomic Force Microscopy*, edited by S. Morita, E. Meyer, and R. Wiesendanger (Springer, New York, 2002).
[47]Nanonis–SPECS Zürich GmbH, 8005 Zürich, Switzerland.
[48]J. Welker, F. de Faria Elsner, and F.J. Giessibl, Appl. Phys. Lett. **99**, 084102 (2011).
[49]J. Rychen *et al*., Rev. Sci. Instrum. **71**, 1695 (2000).
[50]Kolibri-Preamp, SPECS GmbH, Berlin, Germany.
[51]J. Rychen, Doctoral thesis in experimental physics, dissertation ETH No. 14229, Swiss Federal Institute of Technology, Zürich, 2001.
[52]T. Hofmann, J. Welker, and F. J. Giessibl, J. Vac. Sci. Technol. B **28**, C4E28 (2010).
[53]T. Wutscher and F. J. Giessibl, Rev. Sci. Instrum. **82**, 026106 (2011).
[54]M. Lantz *et al*., Science **291**, 2580 (2001).
[55]M. Lantz, H. J. Hug, P. J. A. van Schendel, R. Hoffmann, S. Martin, A. Baratoff, A. Abdurixit, H. J. Guntherodt, and C. Gerber, Phys. Rev. Lett. **84**, 2642 (2000).
[56]C. Barth and M. Reichling, Nature (London) **414**, 54 (2001).
[57]M. Reichling and C. Barth, Phys. Rev. Lett. **83**, 768 (1999).
[58]Y. Sugimoto *et al*., Nat. Mater. **4**, 156 (2005).
[59]Y. Sugimoto *et al*., Nature (London) **446**, 64 (2007).
[60]U. Kaiser, A. Schwarz, and R. Wiesendanger, Nature (London) **446**, 522 (2007).
[61]F. J. Giessibl, Phys. Rev. B **56**, 16010 (1997).
[62]F. J. Giessibl, S. Hembacher, C. Schiller, and J. Mannhart, Nanotechnology **15**, S79 (2004).
[63]S. Torbrügge, J. Lübbe, L. Tröger, M. Cranney, T. Eguchi, Y. Hasegawa, and M. Reichling, Rev. Sci. Instrum. **79**, 083701 (2008).
[64]T. Fukuma *et al*., Rev. Sci. Instrum. **76**, 053704 (2005).
[65]K. Morita, Y. Sugimoto, Y. Sasagawa, M. Abe, and S. Morita, Nanotechnology **21**, 305704 (2010).